Date of resubmission: 05/08/2020

Date of first submission: 03/06/2020

Title: Using DEM to create a CPT based method to estimate the installation requirements of rotary installed piles in sand

Author list

Yaseen Umar Sharif*, Michael John Brown, Matteo Oryem Ciantia, Benjamin Cerfontaine, Craig Davidson, Jonathan Knappett, Gerrit Johannes Meijer, Jonathan Ball

**Corresponding author*

Author details

Yaseen Umar Sharif, MEng
PhD student, School of Science and Engineering, University of Dundee, Fulton Building, Dundee, DD1 4HN, UK
ORCID: 0000-0002-3620-7500
Email: y.u.sharif@dundee.ac.uk

Michael Brown, BEng PhD GMICE
Reader, School of Science and Engineering, University of Dundee, Fulton Building, Dundee, DD1 4HN, UK
ORCID: 0000-0001-6770-4836
Email: m.j.z.brown@dundee.ac.uk

Matteo Oryem Ciantia,
Lecturer, School of Science and Engineering, University of Dundee, Fulton Building, Dundee, DD1 4HN, UK
ORCID: 0000-0003-1897-4471
Email: m.o.ciantia@dundee.ac.uk

Benjamin Cerfontaine, BSc, MSc, PhD
MSCA Research Fellow, School of Science and Engineering, University of Dundee, Fulton Building, Dundee, DD1 4HN, UK
ORCID: 0000-0002-4833-9412
Email: b.cerfontaine@dundee.ac.uk

Craig Davidson, BSc MSc
Research Associate, School of Science and Engineering, University of Dundee, Fulton Building, Dundee, DD1 4HN, UK
ORCID: 0000-0002-4843-5498
Email: c.s.davidson@dundee.ac.uk

Jonathan Adam Knappett, MEng (Hons), PhD
Professor, School of Science and Engineering, University of Dundee, Fulton Building, Dundee, DD1 4HN, UK
ORCID: 0000-0003-1936-881X
Email: j.a.knappett@dundee.ac.uk

Gerrit Johannes Meijer, BSc, MSc, PhD
Postdoctoral Research Associate, School of Science and Engineering, University of Dundee, Fulton Building, Dundee, DD1 4HN, UK
ORCID: 0000-0002-2815-5480
Email: g.j.z.meijer@dundee.ac.uk

Jonathan David Ball, BSc, CGeol, FGS
Chief Geotechnical Engineer, Roger Bullivant Ltd, Burton Upon Trent, UK

Main text word count: 9295

Number of tables: 4

Number of Figures:13

Using DEM to create a CPT based method to estimate the installation requirements of rotary installed piles in sand

Yaseen Umar Sharif*, Michael John Brown, Matteo Oryem Ciantia, Benjamin Cerfontaine, Craig Davidson, Jonathan Knappett, Gerrit Johannes Meijer, Jonathan Ball

Abstract

Deep foundations maybe used in a range of soil types where significant foundation resistance is required but their installation is often associated with disturbance due to noise and vibration. Greater restrictions on use in urban and offshore environments is now commonplace. Screw piles and rotary jacked straight shafted piles are two potential methods of silent piling that could be used as alternative foundation solution, but the effects of certain geometric and installation properties such as installation pitch i.e. the ratio between vertical displacement and rotation, on the required installation torque and force in sand are not well understood. In this paper the effects of installation pitch and base geometry on the installation requirements of a straight shafted pile are simulated in 3D using the discrete element method (DEM). The installation requirements of straight shafted piles into sand have been validated against centrifuge testing, in three different relative densities. The DEM shows reductions in installation force can be achieved by increasing the installation pitch or including a conical tip. An existing cone penetration test (CPT) based prediction method for installation requirements has been improved to include the effects of installation pitch and base geometry for rotary installed piles in sand.

Keywords

DEM, Rotary installation, Silent piling, Installation requirements, CPT

1 Introduction

Deep foundations may be used in a range of soil types where significant foundation resistance is required but, depending on the pile type, their installation may be associated with environmental disturbance due to noise and vibration e.g. in classic pile driving. In the urban environment, noise pollution is usually restricted to specific times of day and vibrational sources are limited in minimum separation from specialist equipment in building such as hospitals and laboratories (BS5228 1992). As well as limitations onshore, legislation and restrictions on the allowable level of noise generated when installing deep foundations have recently been introduced by countries involved in offshore renewable energy development (Huisman 2019). These restrictions are designed to limit the disturbance to marine mammals, but there is a trend to increase foundation size and capacity (Golightly 2014) which may make it more challenging to meet existing and future environmental controls. Therefore, current onshore "silent" piling methods are being investigated to aid in the development of potential offshore "silent" piling techniques.

Several methods have been developed to mitigate the noise problem especially in urban environments through alternative pile construction techniques such as continuous flight auger (CFA) (Mandolini *et al.* 2002), bored displacement piles such as the continuous helical displacement pile (CHD) (Jeffrey *et al.* 2016), the press-in piling method (White and Deeks 2007) and rotary press-in method (Deeks and White 2008) and screw piles (Lutenegger 2009). If current onshore "silent" piling techniques are exported to the offshore environment many factors need to be considered. The CFA and CHD piling method do not lend themselves to offshore installation as both methods require the pile to be cast in-situ using concrete. This limits the available "silent" construction methods to steel displacement piles, such as a tubular piles installed using the press-in or rotary press-in methods or screw piles. In offshore applications the foundation options would be required to resist larger forces, both axially and horizontally. Davidson *et al.*(2020) have suggested that for large jacket structures installed in a water depths up to 80m, an individual pile installed at one corner of a jacket structure

may be required to resist axial compressive and tensile forces of up to 35MN and 26MN respectively, with an associated horizontal load of 6MN. This will result in a need to significantly increase the current sizes of the piles, in terms of both capacity requirements but also structural section sizes. This increase in size raises concerns over the ability to install the steel displacement piles using the aforementioned methods where Davidson *et al.* (2020) suggested vertical installation or crowd forces of up to 22MN in 84% density sand where pitch matched installation of screw piles was used. This raises concerns over the large vertical compressive forces that would be required during installation and practical challenges of creating large capacity load reaction systems in the offshore environment. Thus, where possible it would be advantageous to reduce vertical or crowd installation forces where there is greater ability to control or vary the torque input as required. For example, previous work by Deeks and White (2008) has shown that by using the rotary press-in method and varying the approach to installation, the installation force required to install a tubular pile can be significantly reduced. Both rotary press-in piles and the screw piles are installed in a similar way, through the application of rotational and vertical displacement with the only difference being the addition of helices to the screw pile.

The necessary increase in pile size limits the ability to predict the installation requirements, of both techniques, in terms of torque and vertical force ("crowd force"), which may not be adequately captured by current analytical and empirical based approaches (Davidson *et al*. 2018). In addition to this, the effects of geometry and installation properties such as installation pitch (P_i) (the ratio between vertical ($\dot{w}$) and rotational or angular ($\dot{\theta}$) velocity) (Equation 1) on the required installation torque and force have seen little previous attention.

$$P_i = \frac{\dot{\theta} d_c}{2\dot{w}} \tag{1}$$

were d_c is the diameter of the pile shaft or core. As the geometry of a screw pile is complex, with the addition of helices, this paper will focus on the effect of P_i on the installation requirements of a straight shafted pile.

Currently there are no existing methods focusing on predicting the installation requirements of rotary installed straight shafted piles. Several methods for the predicting installation requirements have been developed for screw piles, with the majority focusing on the prediction of installation torque. Some of these methods split the geometry of the pile into component parts (helix, base and shaft), which allows them to be modified to create a prediction method for the installation requirements of rotary installed straight shafted piles.

For instance Ghaly and Hanna (1991) and Sakr (2015) developed analytical methods for predicting torque which split the installation torque into components based upon geometric features of the screw pile (helices and shaft). These approaches have a tendency to overpredict installation requirements (Davidson *et al.* 2020) and may have limited validation. For example, the Ghaly and Hanna (1991) method, for predicting installation force and torque, was developed through 1g model testing in dry sand and has limited field test verification. The Sakr (2015) procedure has been validated against some limited field scale tests, but with relatively small geometries in comparison to those proposed by Davidson *et al.*(2020).

Prediction methods based upon in-situ cone penetration tests (*CPT*) have been shown to be potentially more reliable, due to the availability of continuous data logging along the path of installation and the full displacement nature of the *CPT* test. Existing *CPT* design methods are typically used to predict the installation torque of screw piles (Gavin *et al.* 2013; Spagnoli 2017; Davidson *et al.* 2018), with a single method proposed for associated installation force by Al-Baghdadi (2017). A common assumption in all of these methods is that the screw piles are installed at P_i that matches the geometric pitch (P_g) of the helix, so that for each rotation the screw pile displaces one P_g vertically. This is referred to as pitch matched or "perfect" installation by Lutenegger (2019). The methods do not consider the effects of P_i on the base and shaft components.

Previous studies on rotary installed straight shafted piles in very dense sands (Deeks and White 2008; Ishihara *et al.* 2015) have shown that by altering the installation pitch, the vertical force required to

install a straight shafted pile can be reduced, but knowledge regarding the effects at other relative densities is limited. Al-Baghdadi (2017) investigated the installation requirements of a straight shafted pile with a conical tip in different relative densities at a single installation pitch. The results showed that the percentage reductions in vertical compressive force with the application of rotation, were density dependent.

Through the use of discrete element modelling (*DEM*) calibrated against triaxial and centrifuge tests, the effect of installation pitch on the installation requirements of straight shafted piles is assessed in this paper and guidance is given on how to optimise the pile geometry and installation pitch in order to reduce the installation requirements. The simulations took place in soils at three different relative densities in sand. Using the results of the simulations, an improvement to the existing *CPT* based design method for predicting installation torque and force proposed by Davidson *et al.* (2018) and Al-Baghdadi (2017) respectively are made to include the effects of varying installation pitch and pile base geometry.

2 Methodology used in discrete element method simulation

The discrete element method (*DEM*) is a numerical modelling framework which can be used to simulate large deformation problems in granular soils (Arroyo *et al.* 2011). Rather than using a continuum to model the soil as finite element analysis (*FEA*) does, the *DEM* uses discrete particles that are able to interact to represent the soil body. *DEM* has been previously used to model a variety of different soil-structure interaction problems including pile plugging (Liu *et al.* 2019), cone penetration tests (Butlanska *et al.* 2014) and jacked piles in sand (Ciantia *et al.* 2019). With the application of an increase gravitational field, the *DEM* is able to act as a virtual centrifuge (Ciantia *et al.* 2018) which when properly calibrated, has the added benefit of using a single soil chamber which can be reset and used multiple times. This allows for direct comparisons to be made in parametric studies and

potentially removes the reliance on specialist laboratory facilities or comparisons to expensive field studies, where soil variability can be an issue with interpretation.

To model the installation of the straight shafted piles, Particle Flow Code 3D 5.0.35 (Itasca Consulting Group 2016) was used alongside a simplified Hertz-Mindlin contact model (Mindlin and Deresiewicz, 1953). The parameters for the soil–soil and soil-structure interaction, were calibrated against laboratory triaxial and centrifuge tests respectively (Sharif *et al.* 2019a) and validated against centrifuge tests of straight shafted piles (Sharif *et al.* 2019b) and screw pile (Sharif *et al.* 2019a) geometries. Further details on the calibration and validation of the contact models used within this study can be found in Sharif *et al* (2019a) and are outlined in Table 1. The sand modelled in the simulations is based upon the properties of HST95, which is a medium to fine well graded sand that is commonly used at the University of Dundee in physical modelling and element testing with the behaviour and properties of the soil being previously investigated and well documented (e.g. Al-Defae *et al.* 2013; Lauder *et al.* 2013). Frictional rigid boundaries (walls) were used to model the straight shafted pile. The model scale pile had a diameter of 10mm, a length of 200mm and a tip with an apex angle of 60 degrees (Figure 1a). Using a gravitational acceleration of 50g, the prototype scale of the pile is 0.5m diameter and an installation depth of 10m. The calculated results from the simulations were scaled in accordance with centrifuge scaling laws (Garnier *et al.* 2007), such that the length is multiplied by N force by $N^2$and torque by N^3, where N is the model scaling factor ($N = 50$). For the DEM implementation of the structure, the pile was split into base and multiple shaft components. The 10 mm diameter model scale *CPT* used within this study was segmented such that it mimicked the instrumentation of a cone penetrometer i.e. there is a “sleeve” of length 4 d_c behind the cone which is used to calculate the sleeve friction (f_s).

The virtual soil chambers for the DEM analysis were created in accordance with the specification in Sharif *et al* (2019b), which implements the particle refinement method (*PRM*) (McDowell *et al.* 2012), which is a similar process to mesh refinement commonly used in *FEA* (Figure 1b). This methodology

148 has previously been implemented by McDowell *et al* (2012) and Shi *et al.*(2019). Three soil chambers
149 were created in this manner each having a different relative density (D_r). The relative densities chosen
150 were 32%, 55% and 73% in line with the centrifuge tests on straight shafted piles conducted by Al-
151 Baghdadi (2017). The dimensions and properties of the soil chambers can be seen in Table 2. To avoid
152 any boundary effects, the radius of the soil chamber was made to be greater than the 20*R* as suggested
153 by Bolton *et al* (1999), where *R* is the radius of the pile. Figure 2 shows the mean effective stress (σ')
154 profile with depth at different radial distances from an installed pile in the dense soil bed. It can be
155 seen that at a radial distance of 20R there is no significant change in mean effective stress compared
156 to the initial soil conditions confirming adequate model sizing.

157 To reduce the run-time of the simulation, a particle size distribution (*PSD*) scaling value (n_i) of 20 was
158 adopted. This value represents the multiplier applied to the diameter of particles, so that each particle
159 now represents n_i^3 particles with the bulk properties of the soil remaining the same. The particle
160 scaling of 20 at the centre of the chamber was selected based upon the minimum recommended ratio
161 of diameter of the pile (d_c) over the median particle size (d_{50}) of 2.69 (Arroyo *et al.* 2011). To limit the
162 possibility of particle migration between scaling zones, the increase in the *PSD* scaling value (n_i),
163 between adjacent concentric zones, was limited to 1.35 for this soil type, such that the smallest
164 particle (d_{00}) of the larger scale is smaller than the median particle in the smaller scale. A maximum n_i
165 of 120 was selected at the boundaries. An example soil chamber can be seen in Figure 1b. Where the
166 shading of the particles represents different values of n_i. The variable scaling values, shown in Figure
167 1b, are consistent across all soil beds used within this study The gravitational field of the chamber was
168 set at 50g to match the centrifuge tests of Al-Baghdadi (2017). Table 3 outlines all of the simulations
169 conducted in this study.

3 Results

3.1 Overview of the reductions in total Installation force and increase in total installation torque with an increase in installation pitch

Figure 3 shows the global reduction in total vertical compressive force and the increase in torque with an increase in installation pitch. A 300-point adjacent averaging of the 80,000 point output data with a reflective end constraint, was used to reduce the level of noise in the outputs from *DEM* simulation, which was produced by the particle scaling. Results show that the total vertical force is reduced, and the total torque is increased as the installation pitch increases. By separating out the contribution of the total force and torque produced by the base and the pile shaft on the straight shafted pile, it is shown (Table 4) that the vertical resistance is primarily produced by the base of the pile and the torque by the shaft for all densities and at all installation pitches. During a monotonic push (P_i = 0), 75% of the vertical force, generated during installation, is attributed to the base of the pile. Therefore, to reduce the installation force in sand, it is much more important to reduce the base component of force rather than the shaft. These effects will be studied in detail in the following section.

3.2 Reduction in installation force due to increase in installation pitch

Consideration of the results is undertaken with a view to improving the shaft and base component terms in the existing *CPT* based installation prediction techniques for rotary pile installation (Al-Baghdadi 2017; Davidson *et al.* 2018) where these methods are broken down into force and torque predictions based upon *CPT* cone resistance (q_c). To assess whether the percentage reduction in vertical force due to varying P_i is consistent across different relative densities, the base resistance (q_b) and the vertical component of shaft resistance (τ_{sv}) (Figure 4) were normalised by the *CPT* cone resistance (q_c) from a 10mm model scale (0.5m prototype scale) virtual CPT conducted in each of the 50g DEM chambers. The normalised resistance was then plotted against P_i (Figure 5). Figure 5a shows that at high installation pitches (P_i >8) the application of rotation causes a 34% reduction in the base

194 resistance. Whereas for the shaft resistance an average decrease of 85% was achieved (Figure 5b) with
195 small variations in normalised shaft resistance occurring between densities. Thus, changing the
196 distribution of total vertical force during rotary installation from 75% to 94% at the base and from 25%
197 to 6% on the shaft.

198 From Figure 5a the reductions in normalised base resistance are consistent across all three relative
199 densities for all installation pitches. At high installation pitches it appears that the normalised base
200 resistance is asymptotic to 0.66 (34% reduction). The asymptote can be used to assess how resistance
201 is produced at the base of the pile during installation. During a monotonic push (P_i = 0) full soil
202 resistance is mobilised and it is assumed that the soil is flowing around the base of the pile as it
203 advances. As the pile advances, frictional resistance would form at the interface of the base and the
204 soil. The vertical component of this shear stress would contribute to q_b. When the pile is rotated (P_i >
205 0), the direction in which the base shear stress (τ_b) acts, rotates accordingly (Figure 4). Thus, the
206 vertical component (τ_{bv}) would reduce, and the tangential component (τ_{bt}) would increase (Figure 4).
207 At high installation pitches (P_i >8) τ_b would act primarily in the tangential direction, with very little
208 frictional/shear resistance acting vertically. This would result in a reduction of q_b, with the percentage
209 reduction representing the proportion of base resistance due to friction. Thus, it can be stated that
210 34% of q_b at P_i =0 is produced through interface friction, for the geometry shown in Figure 1a. The
211 reduction in the base resistance as P_i increases, can be expressed as:

$$\frac{q_b}{q_c} = \frac{1}{\sqrt{1 + (P_i + 2.5)^2}} + b \qquad (2)$$

212 where q_b is the base resistance of the pile, q_c is the cone resistance from a *CPT* and b is the percentage
213 base resistance other than from friction (0.66). Equation 2 appears to capture the reduction in base
214 resistance well (Figure 5a) for all installation pitches and densities.

215 The normalised base resistance results suggest that rotary installing straight shafted piles, at P_i < 4 is
216 not ideal. Low installation pitches in practice are difficult to maintain and appear to yield low

reductions in base resistance. It is much more optimal to install at P_i > 8 as this reduces the base resistance by approximately 34% from the P_i = 0 case.

The normalised shaft resistance (Figure 5b) shows some small variations between the relative densities, with the difference being more apparent at low installation pitches (P_i < 4).As discussed by White and Deeks (2007), the radial stress regime (σ_r) on the pile shaft is caused by unloading of the soil in contact with the shaft, after it has passed around the base of the advancing pile. Jardine *et al* (1993) have shown that the radial stress (σ_r) regime on the shaft of the pile is both density and depth dependent. Therefore, leading to small variations when normalising by q_c. Continuing with the analogy of a displacement pile, at P_i = 0, being similar to *CPT,* the shaft resistance (τ_s) of the pile is comparable to the sleeve friction (f_s) of a *CPT.* τ_s on a displacement pile is commonly defined by equation 3:

$$\tau_s = \sigma_r \tan \delta \tag{3}$$

where τ_s is the shaft resistance, σ_r is the radial stress on the shaft during installation and δ is the interface friction angle. Rearranging Equation 3 gives:

$$\sigma_r = \frac{\tau_s}{\tan \delta} \tag{4}$$

From the *DEM* simulations it can be determined that σ_r on the pile is the same as σ_r on a *CPT* (Figure 4c) as suggested by White and Deeks (2007) and Lehane *et al.* (2005). It is therefore possible to relate τ_s to f_s through σ_r. f_s can be related to q_c through the *CPT* friction ratio ($Fr = f_s/q_c$):

$$\tau_s = f_s \frac{\tan(\delta_{pile})}{\tan(\delta_{CPT})} = a q_c \tan \delta_{pile} \tag{5}$$

$$a = \frac{F_r}{\tan \delta_{CPT}} \tag{6}$$

where a is the stress drop index (Lehane *et al.* 2005; Schneider *et al.* 2007), δ_{CPT} and δ_{pile} are the interface friction angles of the CPT and the pile respectively. Direct comparison between f_s and τ_s is not recommended (White and Deeks 2007), due to the lack of confidence in sleeve friction measurements which may be affected by misalignment and wear over time. From the *CPT*

classification charts proposed by Robertson *et al.* (1986) it is shown that F_r of a *CPT* changes with soil type, but also that small changes in F_r occur in sands of different relative densities, resulting in different values of a. The values of F_r for the *CPT*s from this study range between 0.75% and 1.05%, which results in a 25% difference in the value of the stress drop index. If the shaft resistance is then normalised using $\tau_{sv}/(aq_c\tan\delta_{pile})$ (Figure 5c) the small density effect seen in Figure 5b is removed. The additional data shown in Figure 5c will be discussed at a later stage in this paper.

With the application of rotation (P_i >0), the direction of τ_s is no longer purely vertical. Therefore, the shear stress has both a vertical component (τ_{sv}) and a tangential component (τ_{st}) (Figure 4). τ_{sv} contributes to the vertical force and τ_{st} contributes to installation torque. Assuming σ_r is constant for all values of P_i, in a given density, the relationship between τ_{sv} and P_i can be expressed using simple trigonometry leading to equation 7 (Figure 5c).

$$\frac{\tau_{sv}}{aq_c\tan\delta_{pile}} = \frac{1}{\sqrt{1+{P_i}^2}} \tag{7}$$

As the measurements of *CPT* sleeve friction and therefore F_r are not always considered reliable, as previously discussed, the value of the stress drop index can be assumed to be fixed. In the UWA-05 design method for driven piles in sand (Lehane *et al.* 2005) it is recommended that a=0.03 (F_r=1%) for piles loaded in compression. The fixed value maybe deemed as an acceptable approach as the shaft component of vertical force is small in sand for all installation pitches.

3.3 Increase in installation torque with an increase in installation pitch

As well as considering the vertical force requirements for installation, the existing *CPT* prediction methods also consider torque separately (Davidson *et al.* 2018). Installation torque is generated during rotary installations by a tangential force acting at a lever arm from the centre of the pile (Figure 4). The tangential force is generated by the tangential component of the shear stress at the interface between the pile and soil. To normalise the base component of the installation torque (T_b), T_b is divided by $q_c A_b \overline{R}$ where A_b is the surface area of the base and $\overline{R}$ is the equivalent radius of the pile base. The

shaft component of installation torque (T_s) can be expressed as the tangential component of shear stress acting over the surface area of the shaft (A_s) with a lever arm of the radius of the pile (R). To then normalise the shaft component of torque, T_s is divided by $\tau_s A_s R$, where τ_s is defined by equation 5, A_s is the surface area of the shaft. The normalised base and shaft torque can be seen in Figure 6.

The proportion of the total installation torque that is produced by the base of the pile is relatively low. This is due to the small surface area associated with base geometry and the variable lever arm that increases linearly from 0 to R moving up the pile tip. From the normalised base torque (Figure 6a), all three densities show the same trend. At $P_i > 4$ the value of the normalised torque reaches a limit of 0.34. This agrees with results from the reduction in vertical resistance. Both the normalised base torque and force suggest that 34% of base resistance, for the geometry shown in Figure 1a, during a monotonic push in sand is produced through interface friction. The increase in normalised torque can be expressed as per equation 8 (Figure 6a):

$$\frac{T_b}{q_c A_b \overline{R}} = \frac{(1-b)P_i}{\sqrt{1+P_i^2}} \tag{8}$$

When the normalised shaft torque is plotted against the installation pitch (Figure 6b), a distinct density effect can be seen. The asymptotic value of normalised torque for each density varies. Installation torque is produced through interface friction, which for the shaft is governed by the radial stress that acts on the shaft of the pile. The normalisation method used in Figure 6b applies a variable stress drop index (a) and therefore represents the radial stress that acts on the pile at $P_i = 0$. As the asymptotic value is not 1 for any of the densities, a reduction in radial stress on the shaft of the pile has occurred when it is rotated, and the percentage reduction is density dependent.

3.4 Effect of installation pitch on the radial stress and particle displacement

To assess the change in radial stress along the shaft of the pile, the particle-wall contact forces for each individual section of the segmented pile are assessed at the end of the installation process (Figure 7). The percentage reduction in radial stress on the shaft of the pile installed into the loose soil

chamber is much higher than the percentage reduction of the radial stress in the dense soil. This confirms that the radial stress on the shaft of a pile reduces, if the pile has been rotated, and the percentage reduction of radial stress is density dependant.

The reduction in radial stress is thought to be caused by the rotation of the principle stress, which in turn change the direction of shearing within the soil. This would result in the principal strain direction of the soil to changing accordingly. This has previously been shown in torsional shear tests of hollow cylinder samples of granular material (Tatsuoka *et al.* 1986), where it was shown that the principle strain direction under torsional shearing is inclined between the tangential and vertical direction. In the $Pi = 0$ case the direction of shearing, along the shaft of the pile, is primarily in the vertical direction. Therefore, the principle strain direction is perpendicular to the shaft of the pile, or in other words the soil attempts to move in the radial direction. The soil movement is restricted by the rigid shaft of the pile, resulting in large radial stresses.

When the pile is rotated during installation ($Pi > 0$), the direction of the principle stresses within the soil are assumed to also rotate accordingly. The rotation of the principle stresses results in the direction of shearing no longer being purely in the vertical direction. The direction of shearing when $Pi > 0$ is assumed to be inclined between the vertical and tangential directions. As a result, the principle strain direction would be perpendicular and therefore no longer be purely in the radial direction. The pile would therefore only experience a projection in the radial direction of the stresses induced by the particle displacement. Which ultimately appears as a reduction in the radial stress on the shaft of the pile.

The difference in percentage reduction of the radial stress seen in the different relative densities (Figure 7), is most likely due to the volume of void space and particle packing that is present for a given density, and how this facilitates the movement of particles during shearing. To assess the effect of installation pitch on particle displacement around the pile during installation, the Cartesian coordinates of the individual particles were extracted before and after an imposed vertical

displacement of 0.25 m. The initial location of each particle of interest was then plotted onto a scatter graph and shaded in accordance with its magnitude of displacement in the polar axis being investigated (Figure 8). In loose soil it is much easier for the individual soil particles to displace into a void and for a volume of loose soil to contract under shearing. With the direction of the shear band being inclined, when Pi>0, the soil movement would no longer be restricted by the rigid pile shaft (Figure 8a & b). Which should allow for much more particle displacement to occur in the tangential direction (Figure 8b) and result in a larger reduction in radial stress. In dense soils there is much less void space for particles to displace in to. Therefore, during the shearing process the direction of the shear band has little effect on the principle strain direction (and therefore particle displacement) and the soil dilates to accommodate the volume of the pile (Figure 8c and 8d). As a result, the reduction in radial stress is highly density dependent, with larger reductions occurring in loose soil and smaller reductions in denser soils. This reduction in radial stress during the installation process of rotary installed piles has previously been reported in the centrifuge tests of both Deeks (2008) and Al-Baghdadi (2017). Al-Baghdadi (2017) also suggested that the reduction in radial stress was density dependent with, with denser soils having a lower percentage decrease in radial stress than looser soils, as also shown by the DEM results.

Using the difference in normalised torque from Figure 6b and Figures 7a-7c for the three different soil chambers, it is possible to plot the rotation reduction factor (*f*) against relative density (Figure 7d). The relationship shown in Figure 7d appears linear and can be expressed as:

$$f = 0.73D_r + 0.3 \tag{9}$$

Including *f* in the normalisation of the shaft component of installation torque (Figure 9), removes the density effect seen in Figure 6b. The relationship between T_s and P_i can be expressed by equation 10:

$$\frac{T_s}{afq_cA_sR} = \frac{P_i}{\sqrt{1+{P_i}^2}} \tag{10}$$

The normalised installation torque has shown that at $P_i > 4$ the installation torque does not appear to increase. Whereas for the installation force, the reductions in normalised base resistance becomes asymptotic at $P_i > 8$. Which in practice means it is much more beneficial to install piles at $P_i > 8$ as there is still potential to reduce the installation force without increasing installation torque.

3.5 Comparison of DEM results to previous studies on rotary installed piles

To assess whether the results of the *DEM* simulations give the same relationships as observed in independent physical model tests, the results were compared to the centrifuge tests conducted by Deeks (2008) in very dense sand (D_r = 84%). The pile used in the centrifuge tests was an instrumented close ended flat based pile. To make the results of the DEM simulations comparable to those of Deeks (2008), the normalisation of the base component of installation force and torque no longer uses the cone resistance q_c, as this information is not available for the tests conducted by Deeks (2008). In place of q_c the base resistance of the pile during monotonic push (P_i = 0) is used and notated as $q_{b,0}$. For the shaft, the normalisation can remain the same as τ_s is used by Deeks (2008) which can be expressed as $aq_c tan\delta$. Using equation 9, the radial stress reduction factor can also be obtained for the centrifuge tests, as D_r is known.

The normalised DEM results for the shaft component of installation force and torque are in agreement with the physical model tests (Figure 5c & 9). The relationships between the normalised installation requirements and P_i expressed in equations 7 & 10 fit the trend of the centrifuge tests well. However, when comparing the normalised base components of installation force and torque, a large difference can be seen between the DEM and centrifuge results presented by Deeks (2008) (Figure 10). The DEM simulations show much larger reductions in normalised base resistance during rotary installation, and lower increases in normalised torque. It is assumed that the difference in geometry between the pile used in the centrifuge tests (flat base) and the one used in the DEM simulations (60^o cone) causes the difference in normalised installation requirements.

4 Development of an Analytical model to predict the base component of installation force and torque

With the assumption of normal stress (σ_n) acting along the interface of the pile base, two components contribute to vertical resistance (Figure 4 & 11a). The first contributor is the vertical component of the normal stress. The second is frictional in nature and is the vertical component of the base shear stress (τ_b) induced by σ_n. Assuming that σ_n does not change when the pile is rotated and that τ_b rotates in accordance with the Installation pitch, an analytical solution can be obtained for the installation requirements of the base of the pile. The full derivation of the analytical solution can be seen in the supplementary data for this paper. The variation of force and torque compared to $q_{b,0}$ predicted by the analytical solution can be expressed as:

$$\frac{q_b}{q_{b,0}} = \frac{tan\beta}{tan\beta + tan\delta} + \frac{2tan\delta\, cos\beta}{(tan\beta + tan\delta)\sqrt{cos^2\beta + {P_i}^2} + cos\beta} \tag{11}$$

$$\frac{T_b}{q_{b,0}A_b\overline{R}} = \frac{2tan\beta\, tan\delta}{tan\beta + tan\delta}\left(\left[1 - 2\left(\frac{cos\beta}{P_i}\right)^2\right]\sqrt{1 + \left(\frac{cos\beta}{P_i}\right)^2} + 2\left(\frac{cos\beta}{P_i}\right)^3\right) \tag{12}$$

where β is half of the apex angle of the pile base (Figure 11a). For a flat base β = 90^o and β = 0^o would represent an infinitely tall cone.

To test the applicability of the analytical model (Equations 11 and 12), a series of DEM simulations were conducted using a straight shafted pile with different base geometries in the dense soil chamber. The apex angle of the base of the pile were varied from 20^o to 80^o as well as a flat base case (Table 3). To be able to evaluate the reduction in base resistance when the pile is rotated, each of the piles were installed at P_i = 0 and 4. To compare the base resistance of each pile, a shape function (S) is required. S can be formulated by comparing $q_{b,0}$ to q_c and can be seen in (Figure11b). The relationship between the normalised base resistance and the apex angle appears to be linear and can be expressed as:

$$S = \frac{q_{b,0}}{q_c} = 0.014\beta + 0.55 \quad (13)$$

The results in Figure 11b show that larger apex angles produce much more resistance to penetration, with a flat base having the largest. This is expected as, during full flow conditions, a flat base is assumed to form a cone of sand in front of itself in order to displace the soil radially (White *et al.* 2005). The sand cone would result in soil- soil shear along the interface, which would increase the resistance to installation. A similar phenomenon was also shown in the work of Coyne and Lewis (1999), when investigating seabed ploughs. Their tests showed that nearly double the force was required when laterally displacing a flat wall in comparison to a plough blade with an angle of 40°. This in itself would suggest that to reduce installation force for a rotary installed pile, such as a screw pile, a conical base would be much more beneficial than a flat base.

To deduce the percentage reduction in base resistance for the different geometries when the pile is rotated, q_b of the piles installed at P_i = 4 can be normalised by Sq_c and plotted against the β (Figure 11c). Figure 11c shows that smaller apex angles, have larger scope for reduction in vertical resistance. The analytical model for the reduction in vertical resistance (Equation 11) shows a good comparison to DEM results (Figure 11c), although the DEM results show a small variation against the analytical model for the flat base. The analytical solution expressed in equation 11 assumes that there is no loss in normal stress when the pile is rotated and reductions in vertical base resistance only occur on the vertical component of shear stress. For a flat base the normal stress is perpendicular to the surface of the base and therefore there is no vertical component of shear stress. If there is no vertical component to τ_b then the analytical model will result in no reductions in base resistance. As a result, Equation 11 is unable to predict the reduction in vertical base resistance for a flat base, which is seen in both the DEM and centrifuge tests of Deeks (2008). The most likely explanation for the reduction in base resistance for the flat base is a change in geometry of the soil cone (as shown in Figure 12) when the pile is rotated compared to a monotonic push, as proposed by Deeks (2008). Figure 12 shows the magnitude of average particle displacement (U) for a flat based pile, installed at P_i = 0 and 4. For the

P_i = 0 case the shape of the nose cone is conical in nature and extends vertically by 2 d_c and radially by 1.5 d_c. In contrast to this the nose cone of the pile installed at P_i = 4, the vertical and radial extent of the nose cone are 1.6 d_c and 2.0 d_c respectively. It is therefore recommended that the analytical solution is not used to predict the reduction in base resistance for a flat base and a 10% reduction in base resistance for piles installed at P_i > 4 is used for flat based piles. This though needs further investigation.

As equation 11 appears to successfully predict the reduction in vertical base resistance due to rotation for the conical tip of different apex angles, it was then compared to the results of the 60° cone installed using DEM at different installation pitches (Figure 11d). The analytical equation fits the results well, for the conical tip. It should also be noted that as previously discussed the analytical model is unable to predict the reductions of the flat base due to a potential difference in mechanism. Thus, showing that by changing the base of the pile from a flat base to a 60° conical tip and rotary installing at P_i > 8, a reduction in base resistance of 67% is possible (Figure 11c &d).

The proposed analytical model predicts the increase in the base component of the installation torque (Equation 12). Similar to Equation 11, Equation 12 compares the base torque to $q_{b,0}$. To normalise the base component of torque in terms of q_c, S is required. Figure 11e shows the normalised base torque against β. The results show that with an increase in apex angle, there is an increase in normalised torque, which agrees with the analytical solution in Equation 12. Although the normalised torque is low for small apex angles, the value of base torque is larger than the torque for the shallow apex angles. This is due to the increased surface area associated with small apex angles. It can also be seen in Figure 11e, that the normalised base torque for the flat base matches the centrifuge test of Deeks (2008). Figure 11f shows that Equation 12 is able to capture the behaviour of the normalised torque for the 60° cone installed at different installation pitches.

The analytical solutions (Equation 11 & 12) compare well with the DEM, with only the flat base, from both DEM and the centrifuge tests, showing some small variations against the analytical model. The

results show that it is possible to reduce the base resistance significantly by changing from a flat base to a conical tip. The conical tip will increase the base component of installation torque, but the base component remains relatively low in comparison with the shaft contribution to installation torque.

5 Modification of the CPT prediction method to incorporate installation pitch and base geometry

Using the relationships obtained through this investigation it is now possible to modify the base and shaft components of the *CPT* based prediction method for installation torque and installation force originally proposed by Davidson *et al.* (2018) and Al-Baghdadi (2017), respectively. The updated equations include additional terms to add the effects of installation pitch and base geometry. The installation torque can be predicted using the following equations:

$$T = T_b + T_s \tag{14}$$

$$T_b = \overline{q_c} S \pi \frac{{d_c}^3}{12 \sin\beta} \frac{tan\beta\ tan\delta}{tan\beta + tan\delta} \left(\left[1 - 2\left(\frac{cos\beta}{P_i}\right)^2 \right] \sqrt{1 + \left(\frac{cos\beta}{P_i}\right)^2} + 2\left(\frac{cos\beta}{P_i}\right)^3 \right) \tag{15}$$

$$T_s = \sum_{\Delta x = 1}^{\Delta xi = L} a \overline{q_c} \tan\delta \pi \Delta x d_c \frac{P_i}{\sqrt{1 + {P_i}^2}} f \tag{16}$$

$$f = 0.63 D_r + 0.52 \tag{17}$$

$$a = \frac{F_r}{\tan\delta} \tag{18}$$

$$P_i = \frac{\dot{\theta} d_c}{2\dot{w}} \tag{19}$$

$$S = 0.013\beta + 0.6 \tag{20}$$

where T is the total torque resulting during installation, T_b is the torque associated with the base of the pile, T_s is the torque associated with the shaft of the pile, $\overline{q_c}$ is the average value of q_c over a depth

of $3d_c$ ($1.5d_c$ above and below), β is half of the apex angle of the pile tip (for a flat base β=90°) and *S* is the shape function for the base of the pile.

To predict the installation force the following equations are used:

$$F = F_b + F_s \tag{21}$$

$$F_b = \overline{q_c}\, S\pi \frac{{d_c}^2}{4}\left(\frac{tan\beta}{tan\beta + tan\delta} + \frac{2tan\delta\, cos\beta}{(tan\beta + tan\delta)\sqrt{cos^2\beta + {P_i}^2} + cos\beta}\right) \tag{22}$$

$$F_s = \sum_{\Delta x = 1}^{\Delta xi = L} \overline{aq_c} \tan(\delta)\pi \Delta x d_c \frac{1}{\sqrt{1 + {P_i}^2}} \tag{23}$$

where *F* is the total force encountered during installation, F_b is the force attributed to the base of the pile, F_s is the force generated through shear resistance on the shaft of the pile. When calculating the base resistance for a rotary installed pile with a flat base, a 10% reduction in q_b should be considered in place of Equations 22 for piles installed at P_i > 4. This is due to the analytical solution used to formulate Equation 22 being unable to capture the behaviour of the flat base. The installation requirements for the shaft are calculated from the sum of intervals of length Δ*x* (Figure 1a) over the total length of the pile. Although *f* should be present in Equation 23, the parameter has been omitted for simplicity. This is due to the negligible contribution of the shaft to the installation force at P_i>1 (Table 4).

5.1 Model-scale pile torque and force predictions

The proposed methods were used to predict the installation torque and force of a model pile installed in medium dense HST95 sand. The installation pitch of the 50g centrifuge test was 3.97 and the total torque and force were recorded with depth. The pile was 200 mm in length with an apex angle of 60°. *CPT* cone resistance data in the same density of sand was recorded in the centrifuge tests and can be seen in Figure 13a. Figure 13b&c shows the comparison between the predicted and measured values for both Installation force and torque. The predictions using the proposed equations show a good correlation with the measured values for both the torque and force, predictions using the original

equations reported in Al-Baghdadi (2017) and Davidson *et al*. (2018) can also be seen to over predict installation requirements (Figure 13b&c). Showing that the proposed changes to the CPT installation prediction method are better at predicting installation requirements.

6 Conclusions

The introduction of restrictions upon the allowable level of noise generated when installing deep foundations offshore has increased the demand for "silent" piling techniques to be developed for the offshore environment. One potential onshore silent piling technique that may be exported offshore is the rotary installation of steel displacement piles, such as the rotary press-in method for tubular piles or the installation of screw piles. Methods for predicting the installation requirements of rotary installed straight shafted piles are limited, although several have previously been developed for small scale onshore screw piles which may not be adequate for larger geometries. The effect of installation pitch and base geometry, on the base and shaft components of installation force and torque has been investigated for straight shafted piles in multiple relative densities using the *DEM* technique. The *DEM* simulations conducted within this paper have been calibrated and validated against physical triaxial and centrifuge tests.

From the investigation it can be concluded that it is possible to significantly reduce the vertical installation force (or crowd) of a straight shafted pile by increasing the installation pitch in all relative densities. Simulations conducted on a straight shafted pile with an apex angle of 60^{o}, showed a reduction in vertical base and shaft resistance of 34% and 85% respectively at $P_i > 8$. The installation torque that is generated when the pile is rotated, is primarily produced by the shaft of the pile. The installation torque increases with installation pitch although the increase in installation torque is negligible at $P_i > 4$. Therefore, it is much more beneficial for rotary installed piles to be installed at $P_i > 8$. A reduction in shaft resistance during installation was discovered, with the percentage reduction being larger in loose soil and much smaller in denser soils.

476 Comparisons against independent centrifuge tests highlighted that the geometry of the pile base
477 affected the base components of installation torque and force. Flat based piles were found to increase
478 the resistance to penetration by nearly double when installed through the press in method (no
479 rotation). Moreover, the percentage reduction in installation force and increase in installation torque
480 during rotary installation are significantly influenced by the base geometry. This led to the
481 development of an analytical solution for predicting the change in the base component of the
482 installation requirements for conical base geometries. It was found that 40^o is the optimum apex angle
483 for the base of the pile, reducing the installation force significantly while maintaining a relatively low
484 torque.

485 Using the results of the DEM simulations and the analytical model, modifications to the base and shaft
486 components of the existing *CPT* based predictions methods for installation torque and force proposed
487 by Davidson *et al.* (2018) and Al-Baghdadi (2017) respectively have been improved to include the
488 effects of varying installation pitch and pile base geometry. The improved method will aid in the
489 prediction of the installation requirements and plant development for large offshore "silent" pile
490 deployment.

491

492 7 Acknowledgements

493 This research is a part of an EPSRC NPIF funded studentship with Roger Bullivant Limited The 4th
494 author is supported by the European Union's Horizon 2020 research and innovation programme under
495 the Marie Skłodowska-Curie grant agreement No 753156. The authors would also like to acknowledge
496 the support of EPSRC (Grant no. EP/N006054/1: Supergen Wind Hub: Grand Challenges Project: Screw
497 piles for wind energy foundations).

498

Table captions

Table 1: HST95 sand physical and numerical properties (Sharif et al 2019a)

Table 2: Properties of the virtual soil chambers used in this study at different relative densities

Table 3: Overview of simulations conducted in this study.

Table 4: Percentage contribution to installation requirements from base and shaft for all soil densities

Figure captions

Figure 1: a)Schematic of the geometry of the pile used by (Al-Baghdadi 2017) and in the DEM simulations (model scale dimensions in brackets) b) Example soil chamber used in DEM simulations, shading indicates the particle size distribution scaling applied, diameter 25 m (0.5m), height 20 m (0.4m) and Dr = 73% (gravitational acceleration 50g).)

Figure 2: Mean effective stress with depth below ground level at different radial distances from an installed pile (P_i =0 D_r = 73%).

Figure 3: Comparison of DEM results for medium dense sand at varying installation pitch, a) total vertical force vs penetration depth, b) total torque vs penetration depth

Figure 4: Schematic diagram of a rotary installed pile, showing the component and direction of shear stresses acting on a straight shafted pile during rotary installation.

Figure 5: Comparison of normalised vertical stress results versus increasing installation pitch a) normalised base resistance (q_b/q_c) b) Normalised shaft resistance (τ_{sv}/q_c) c) Comparison of the radial stress distribution along the shaft of an installed pile and CPT in the dense soil bed (D_r = 73%) d) Comparison of equation 7 to the normalised shaft resistance from DEM and independent centrifuge tests of Deeks (2008).

Figure 6: Normalised installation torque vs installation pitch a) base component of torque b) shaft component of torque.

Figure 7: Comparison of normalised radial stress on the pile shaft for various installation pitches a) loose b) medium dense c) dense d) Rotation reduction factor for radial stress on the pile shaft vs relative density.

Figure 8: Comparison of particle displacement during installation at P_i = 0 & 4 for 0.25m of pile vertical movement. (Particles are shaded by displacement in polar axis) a) Loose soil bed radial displacement b) Loose soil bed rotational displacement c) Dense soil bed radial displacement d) Dense soil bed rotational displacement

Figure 9: Comparison of normalised shaft resistance from DEM and independent centrifuge test of Deeks (2008), with the inclusion of the rotation reduction factor, to Equation 10.

Figure 10: Comparison of base component of installation requirements between DEM and independent centrifuge tests of Deeks (2008) a) Installation force b) Installation torque

Figure 11: Comparison of equation 11 and 12 to DEM and independent centrifuge tests of Deeks (2008) a) Diagram of possible tip geometries b) normalised base resistance for pushed in pile with different base geometries c) normalised base resistance against pile tip angle,β d) normalised base resistance against installation pitch e) normalised base torque against pile tip angle, β f) normalised base torque against installation pitch.

Figure 12 Average particle displacement below the base of an advancing flat based pile. a) Installation pitch = 0, b) Installation pitch = 4.

Figure 13: Prediction of installation requirements of a rotary installed straight shafted pile. Installed at P_i = 3.97 in centrifuge test from CPT Cone tip resistance, a) CPT Cone tip resistance from CPT conducted in the geotechnical centrifuge (D_r = 55%), b) Predicted vs measured prototype installation force, c) Predicted vs measured prototype Installation torque.

References

Al-Baghdadi, T. 2017 *Screw piles as offshore foundations : Numerical and physical modelling*. Ph.D. thesis, School of Science and Engineering, University of Dundee, Dundee, U.K.

Al-Defae, A. H., Caucis, K. and Knappett, J. A. 2013 'Aftershocks and the whole-life seismic performance of granular slopes', *Géotechnique*, 63(14), pp. 1230–1244. doi: 10.1680/geot.12.P.149.

Arroyo, M., Butlanska, J., Gens, A., Calvetti, F. and Jamiolkowski, M. 2011 'Cone penetration tests in a virtual chamber', *Géotechnique*, 61(6), pp. 525–531. doi: 10.1680/geot.9.P.067.

Bolton, M. D., Gui, M. W., Garnier, J., Corte, J. F., Bagge, G., Laue, J. L. and Renzil, R. 1999 'Centrifuge cone penetration tests in sand', *Géotechnique*, 49(4), pp. 543–552. doi: 10.1680/geot.1999.49.4.543.

BS5228 1992 *Noise control on construction and open sites - Part 4: Code of practice for noise and vibration control applicable to piling operations*. London, United Kingdom, British Standards Institute.

Butlanska, J., Arroyo, M., Gens, A. and O'Sullivan, C. 2014 'Multiscale analysis of CPT in a virtual calibration chamber', *Canadian Geotechnical Journal*, 26(1), pp. 80–86. doi: 10.1139/cgj-2012-0476.

Ciantia, M. O., Boschi, K., Shire, T. and Emam, S. 2018 'Numerical techniques for fast generation of large discrete-element models', *Proceedings of the Institution of Civil Engineers - Engineering and Computational Mechanics*, 171(4), pp. 147–161. doi: 10.1680/jencm.18.00025.

Ciantia, M. O., O'Sullivan, C. and Jardine, R. 2019 'Pile penetration in crushable soils: Insights from micromechanical modelling', in *XVII European Conference on Soil Mechanics and Geotechnical Engineering-2019*. Reykjavik, Iceland, 1-6 September 2019 pp. 298–317. doi: doi: 10.32075/17ECSMGE-2019-1111.

Coyne, J. C. and Lewis, G. W. 1999 'Analysis of plowing forces for a finite-width blade in dense, ocean bottom sand', in *Oceans '99 Ridimg the Crest into the 21st Century*. Seattle WA, USA: IEEE, pp. 1–10.

568 Davidson, C., Al-Baghdadi, T., Brown, M. J., Brennan, A., Knappett, J., Augarde, C. E., Coombs, W.,
569 Wang, L., Richards, D., Blake, A. and Ball, J. 2018 'A modified CPT based installation torque prediction
570 for large screw piles in sand', *In* 4th *International Symposium on Cone Penetration Testing*. Delft,
571 Netherlands, 21-22 June 2018. CRC Press, pp. 255–261. doi:
572 https://doi.org/10.1201/9780429505980.

573 Davidson, C., Brown, M. J., Cerfontaine, B., Knappett, J. A., Brennan, A. J., Al-Baghdadi, T., Augarde,
574 C., Coombs, W., Wang, L., Blake, A., Richards, D. and Ball, Jonathan, D. 2020 *Feasibility of screw piles*
575 *for offshore jacket structures*, *Géotechnique Accepted subject to revision (03/07/20)*.

576 Deeks, A. D. 2008 *An investigation into the strength and stiffness of jacked piles in sand*. Ph.D. thesis,
577 Department of Engineering, University of Cambridge, Cambridge, U.K.

578 Deeks, A. D. and White, D. 2008 'Centrifuge modelling of rotary jacked tubular piles "Gryopiling"', *In*
579 *Proceedings of the second BGA International Conference on Foundations ICOF2008*. Dundee, United
580 Kingdom, 24 June 2008. Bre Press, pp. 531–544.

581 Garnier J, Gaudin, C., Springman, S. M., Culligan P, Goodings, D., Konig, D., Kutter, B., Phillips, R.,
582 Randolph, M. and Thorel, L. 2007 'Catalogue of scaling laws and similitude questions in geotechnical
583 centrifuge modelling', *International Journal of Physical Modelling in Geotechnics*, 7(3), pp. 1–23.

584 Gavin, K., Doherty, P. and Spagnoli, G. 2013 'Prediction of the installation torque resistance of large
585 diameter helical piles in dense sand.', *In* 1st *International Geotechnical Symposium on Helical*
586 *Foundations.* Amherst, USA,8-10 August 2013, pp. 131–140.

587 Ghaly, A. and Hanna, A. 1991 'Experimental and theoretical studies on installation torque of screw
588 anchors', *Canadian Geotechnical Journal*, 28(3), pp. 353–364. doi: 10.1139/t91-046.

589 Golightly, C. 2014 'Technical Paper : Tilting of monopiles Long, heavy and stiff, pushed beyong their
590 limits', *Ground Engineering*, January, pp. 20–23.

591 Huisman, M. 2019 'Silent Foundation Concept: Helical Piles For Skirt and Pre-piled Jacket

592 Foundations', *In* International Symposium on Screw Piles for Energy Applications. Dundee, United
593 Kingdom, 27-28 May 2019. University of Dundee, pp. 117–118. doi: 10.20933/100001123.

594 Ishihara, Y., Haigh, S. and Bolton, M. 2015 'Estimating base resistance and N value in rotary press-in',
595 *Soils and Foundations*. 55(4), pp. 788–797. doi: 10.1016/j.sandf.2015.06.011.

596 Itasca Consulting Group, I. 2016 'PFC 5.0'. Minneapolis: Itasca Consulting Group, Inc.

597 Jardine, R. J., Lehane, B. M. and Everton, S. J. 1993 'Friction Coefficients for Piles in Sands and Silts',
598 *Offshore Site Investigation and Foundation Behaviour*, 28(1), pp. 661–677. doi: 10.1007/978-94-017-
599 2473-9_31.

600 Jeffrey, J. R., Brown, M. J., Knappett, J. A., Ball, J. D. and Caucis, K. 2016 'CHD pile performance: part I
601 – physical modelling', *Proceedings of the Institution of Civil Engineers - Geotechnical Engineering*,
602 169(5), pp. 421–435. doi: 10.1680/jgeen.15.00131.

603 Lauder, K. D., Brown, M. J., Bransby, M. F. and Boyes, S. 2013 'The influence of incorporating a
604 forecutter on the performance of offshore pipeline ploughs', *Applied Ocean Research*, 39, pp. 121–
605 130. doi: 10.1016/j.apor.2012.11.001.

606 Lehane, B. M., Schneider, J. . and Xu, X. 2005 'The UWA-05 method for prediction of axial capacity of
607 driven piles in sand', *In Proceedings of the International Symposium on Frontiers in Offshore*
608 *Geotechnics* Perth, Australia, 19-21 September 2005, CRC Press. pp. 683–689.

609 Liu, J., Duan, N., Cui, L. and Zhu, N. 2019 'DEM investigation of installation responses of jacked open-
610 ended piles', *Acta Geotechnica 14*., pp. 1805-1819. doi: 10.1007/s11440-019-00817-7.

611 Lutenegger, A. J. 2009 'Cylindrical shear or plate bearing - Uplift behavior of multi-helix screw
612 anchors in clay', in *Geotechnical Special Publication*, pp. 456–463. doi: 10.1061/41021(335)57.

613 Lutenegger, A. J. 2019 'Screw Piles and Helical Anchors- What we Know and What we Don't Know:
614 An Academic Perspective - 2019', *In* International Symposium on Screw Piles for Energy Applications.

615 Dundee, United Kingdom, 27-28 May 2019. University of Dundee, pp. 15–28. doi:
616 10.20933\100001123.

617 Mandolini, A., Ramondini, M., Russo, G. and Viggiani, C. 2002 'Full scale loading tests on
618 instrumented CFA piles', In *International Deep Foundations Congress, Orlando, Florida, 14-16*
619 *February 2002*, pp. 1088–1097. doi: 10.1061/40601(256)77.

620 McDowell, G. R., Falagush, O. and Yu, H.-S. 2012 'A particle refinement method for simulating DEM
621 of cone penetration testing in granular materials', *Géotechnique Letters*, 2(3), pp. 141–147. doi:
622 10.1680/geolett.12.00036.

623 Mindlin, R. D. and Deresiewicz, H. 1953 'Elastic spheres in contact under varying oblique forces',
624 *Journal of Applied Meechanics ASME*, 20, pp. 327–344. doi: 10.1007/978-1-4613-8865-4_35.

625 Robertson, P. K., Campanella, R. G., Gillespie, D. and Greig, J. 1986 'Use of piezometer cone data', In
626 *ASCE Speciality Conference In Situ 1986*. Blacksburg, USA, 23-25 June 1986. pp. 1263–1280.

627 Sakr, M. 2015 'Relationship between Installation Torque and Axial Capacities of Helical Piles in
628 Cohesionless Soils', *Journal of Performance of Constructed Facilities*, 29(6), p. 04014173. doi:
629 10.1061/(ASCE)CF.1943-5509.0000621.

630 Schneider, J., Engineer, C. and White, D. J. 2007 'Back analysis of Tokyo port bay bridge pipe pile load
631 tests using piezocone data', In *International Workshop on Recent Advances in Deep Foundations*.
632 Yokosuka, Japan, 1-2 February 2007. pp. 183–194. doi: 10.1201/9780203938416.ch11.

633 Sharif, Y., Brown, M. J., Ciantia, M., Knappett, J., Davidson, C., Cerfontaine, B., Robinson, S. and Ball,
634 J. 2019a 'Numerically Modelling the Installtion and loading of Screw Piles using DEM', *In*
635 *International Symposium on Screw Piles for Energy Applications*. Dundee, United Kingdom, 27-28
636 May 2019. University of Dundee, pp. 101–108. doi: 10.20933/100001123.

637 Sharif, Y., Ciantia, M., Brown, M. J., Knappett, J. A. and Ball, J. D. 2019b 'Numerical Techniques For
638 the Fast Generation of Samples Using the Particle Refinement Method', In *Proceedings of the 8th*

International Conference on Discrete Element Methods. Enschede, Netherlands, 21-26 July 2019, p. 181.

Shi, D., Yang, Y., Deng, Y. and Xue, J. 2019 'DEM modelling of screw pile penetration in loose granular assemblies considering the effect of drilling velocity ratio', *Granular Matter*. 21(3), pp. 1–16. doi: 10.1007/s10035-019-0933-3.

Spagnoli, G. 2017 'A CPT-based model to predict the installation torque of helical piles in sand', *Marine Georesources and Geotechnology*, 35(4), pp. 578–585. doi: 10.1080/1064119X.2016.1213337.

Tatsuoka, F., Sonoda, S., Hara, K., Fukushima, S. and Pradhan, T. B. S. 1986 'Failure and Deformation of Sand in Torsional Shear', *Soils and Foundations*, 26(4), pp. 79–97. doi: doi.org/10.3208/sandf1972.26.4_79.

White, D. J. and Deeks, A. D. 2007 'Recent research into the behaviour of jacked foundation piles', *In International Workshop on Recent Advances in Deep Foundations*. Yokosuka, Japan, 1-2 February 2007, pp. 3–26. doi: 10.3101/1098-7096(2007)68.

White, D., Schneider, J. and Lehane, B. 2005 'The influence of effective area ratio on shaft friction of displacement piles in sand', *In Proceedings of the International Symposium on Frontiers in Offshore Geotechnics* Perth, Australia, 19-21 September 2005, CRC Press. pp. 741–747.

Notation

a	Stress drop index
b	percentage base resistance other than from friction
A_b	Surface area of pile base
A_s	Surface area of pile shaft
CFA	Continuous flight auger pile
CHD	Continuous helical displacement pile
CPT	Cone penetration test
d_{00}	Minimum particle size
d_{50}	Median particle size
d_{100}	Maximum particle size
d_c	Diameter of pile core
DEM	Discrete element modelling
D_r	Relative density
f	Radial stress reduction factor
F	Total Installation force
FEA	Finite element analysis
F_b	Installation force from base
F_h	Installation force from helix
F_r	CPT friction ratio
F_s	Installation force from shaft
f_s	Sleeve friction
k_0	Coefficient of earth pressure at rest
L	Length of the pile
n_i	Particle scaling value
N	Model scaling factor
P_g	Geometric pitch
P_i	Installation pitch
PRM	Particle refinement method
PSD	Particle size distribution
q_b	Base resistance
$q_{b,0}$	Base resistance of pile installed at $P_i = 0$
$\underline{q_c}$	CPT cone resistance
q_c	average q_c over $3d_c$
q_{ca}	average CPT cone resistance
R	Radius of the pile
$\overline{R}$	average radius of cone
S	Shape function for pile base
T	Total installation torque
T_b	Base component of installation torque
T_h	Torque from helix
T_{h1}	Torque from lower surface of helix

T_{h2}	Torque from outer perimeter of helix
T_{h3}	Torque from leading edge of helix
T_s	Shaft component of installation torque
U	Magnitude of average particle displacement
$\dot{w}$	Vertical velocity of pile
X	Horizontal distance from pile centre
y	Depth below ground level
z	Penetration depth
β	Half of the apex angle of pile base
γ'	Effective unit weight of soil
δ	Interface friction angle
δ_r	Particle radial displacement
δ_{CPT}	Critical state friction angle of the CPT
δ_{Pile}	Critical state friction angle of the Pile
δ_θ	Particle rotational displacement
$\dot{\theta}$	Rotational velocity
σ'	Mean effective stress
σ_r	Radial stress on the shaft of the pile
σ_n	Normal stress on interface of pile base
τ_b	Base shear stress
τ_{bt}	Tangential component of base shear stress
τ_{bv}	Vertical component of base shear stress
τ_s	Shaft shear stress
τ_{st}	Tangential component of shaft shear stress
τ_{sv}	Vertical component of shaft shear stress

Table 1: HST95 sand physical and numerical properties (Sharif et al 2019a)

HST95 silica sand property	Value
Physical properties	
Sand unit weight γ (kN/m^3)	16.75
Minimum dry density γ_{max} (kN/m^3)	14.59
Maximum dry density γ_{min} (kN/m^3)	17.58
Critical state friction angle, φ (degrees)	32
Interface friction angle, δ (degrees)	18
D_{30} (mm)	0.12
D_{60} (mm)	0.14
DEM Parameters	
Shear modulus, G (GPa)	3
Friction coefficient, μ (-)	0.264
Poisson's ratio, ν (-)	0.3
Interface friction coefficient [pile], μ_{pile} (-)	0.16

Table 2: Properties of soil chambers used in this study at different relative densities (model scale parameters)

Property	Loose	Medium Dense	Dense
Relative Density (%)	**32**	**55**	**72**
Voids ratio (e)	**0.67**	**0.60**	**0.55**
Height (mm)	**400**	**400**	**400**
Radius (mm)	**250**	**250**	**250**
Core PSD scaling (N_c)	**20**	**20**	**20**
Gravitational field	**50**	**50**	**50**
Number of Particles	**200,000**	**225,000**	**250,000**
Pile Diameter (mm)	**10**	**10**	**10**
Cone penetrometer Diameter(mm)	**10**	**10**	**10**

Table 3: Overview of simulations conducted in this study

Test Number	Pile type	Relative density, D_r (%)	Installation Pitch, P_i (-)	tip geometry (degrees)	β (degrees)
1	CPT	32	0	60	NA
2	Straight shafted pile	32	0	60	30
3	Straight shafted pile	32	0.5	60	30
4	Straight shafted pile	32	1	60	30
5	Straight shafted pile	32	4	60	30
6	Straight shafted pile	32	8	60	30
7	Straight shafted pile	32	10	60	30
8	CPT	55	0	60	NA
9	Straight shafted pile	55	0	60	30
10	Straight shafted pile	55	0.5	60	30
11	Straight shafted pile	55	1	60	30
12	Straight shafted pile	55	4	60	30
13	Straight shafted pile	55	8	60	30
14	Straight shafted pile	55	10	60	30
15	CPT	73	0	60	NA
16	Straight shafted pile	73	0	60	30
17	Straight shafted pile	73	0.5	60	30
18	Straight shafted pile	73	1	60	30
19	Straight shafted pile	73	4	60	30
20	Straight shafted pile	73	8	60	30
21	Straight shafted pile	73	10	60	30
22	Straight shafted pile	73	0	20	10
23	Straight shafted pile	73	0	40	20
24	Straight shafted pile	73	0	80	40
25	Straight shafted pile	73	0	180 (flat)	90
26	Straight shafted pile	73	4	20	10
27	Straight shafted pile	73	4	40	20
28	Straight shafted pile	73	4	80	40
29	Straight shafted pile	73	4	180 (flat)	90

Table 4: Percentage contribution to installation requirements from base and shaft for all soil densities

Installation Pitch	Installation Force F		Installation Torque T	
	Base (%) F_b	Shaft F_s (%)	Base T_b (%)	Shaft T_s (%)
0	75	25	0	0
0.5	80	20	39	61
1	82	18	37	63
4	90	10	38	62
8	94	6	40	60
10	95	5	39	61

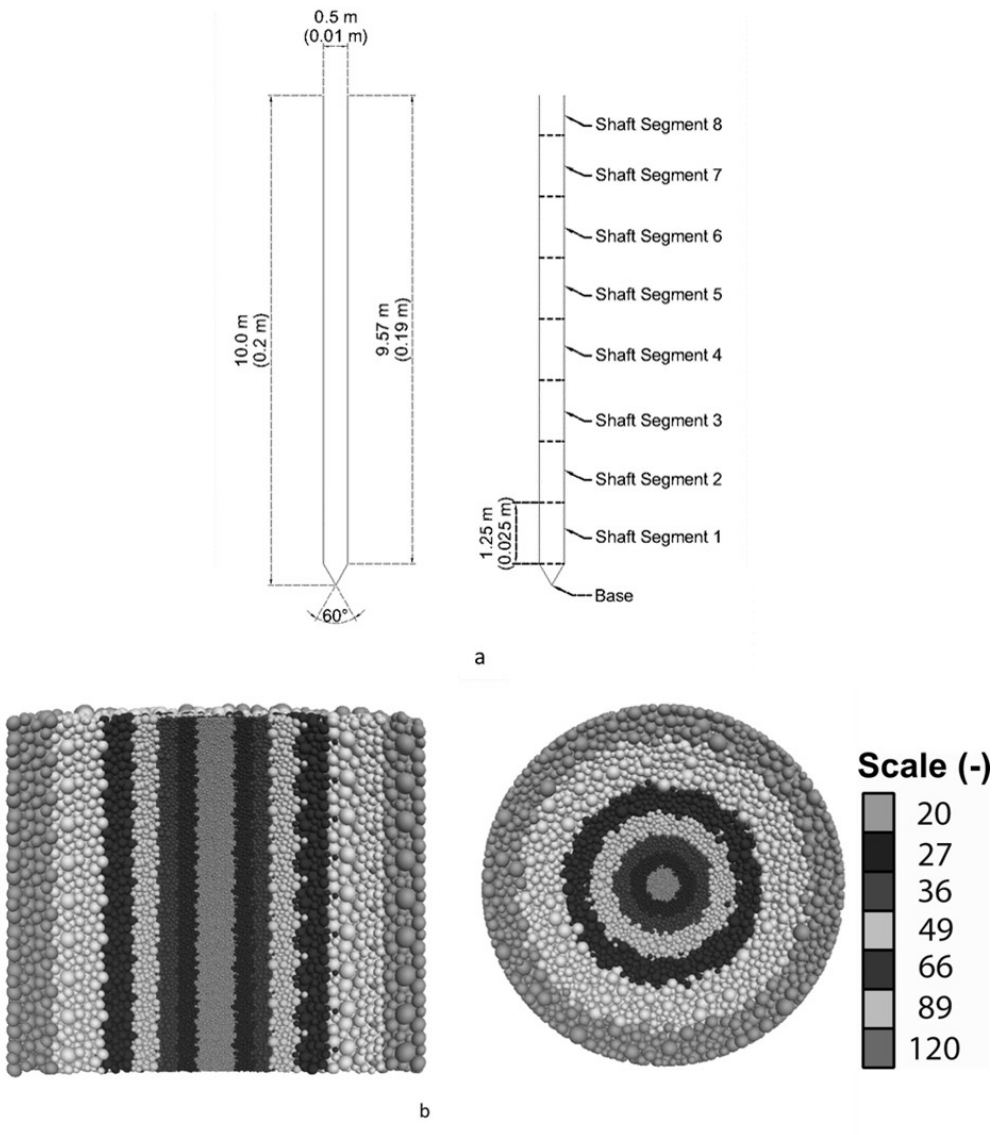

Figure 1: a)Schematic of the geometry of the pile used by (Al-Baghdadi 2017) and in the DEM simulations (model scale dimensions in brackets) b) Example soil chamber used in DEM simulations, shading indicates the particle size distribution scaling applied, diameter 25 m (0.5 m), height 20 m (0.4 m) and D_r = 73% (gravitational acceleration 50g)

159x181mm (150 x 150 DPI)

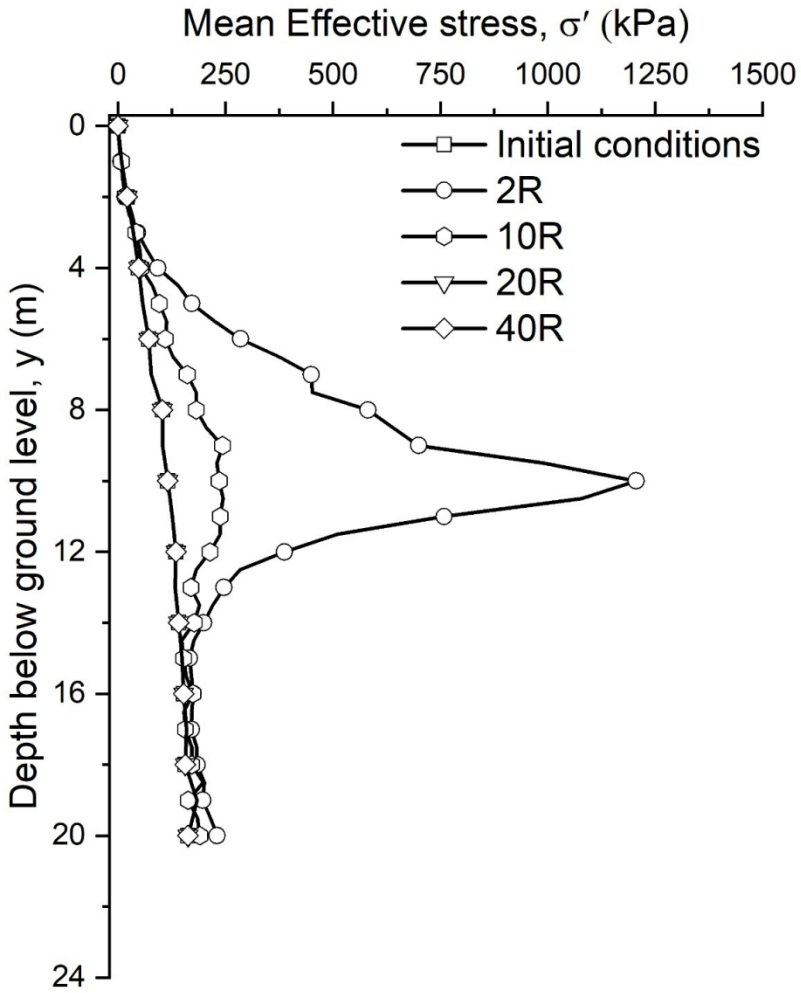

Figure 2: Mean effective stress with depth below ground level at different radial distances from an installed pile (P_i =0 D_r = 73%).

159x198mm (220 x 220 DPI)

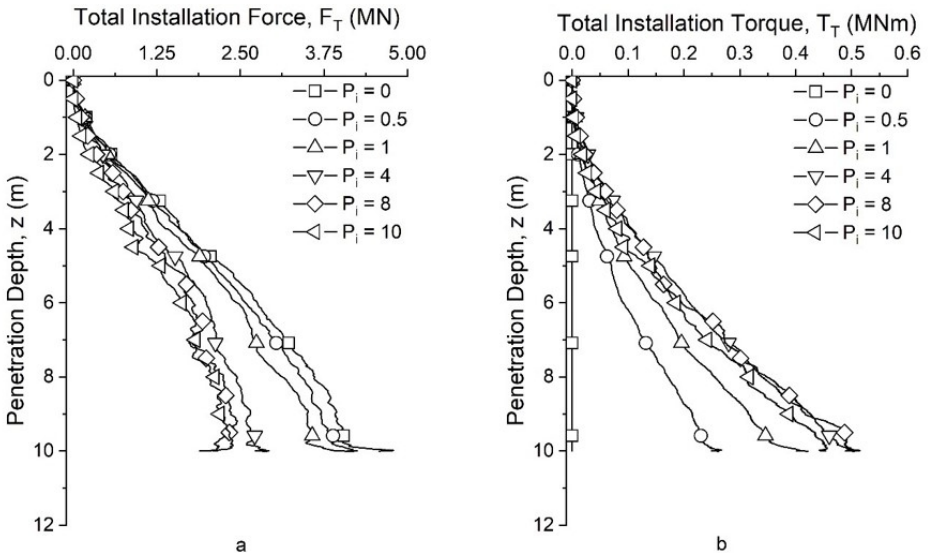

Figure 3: Comparison of DEM results for medium dense sand at varying installation pitch, a) total vertical force vs penetration depth, b) total torque vs penetration depth

158x98mm (150 x 150 DPI)

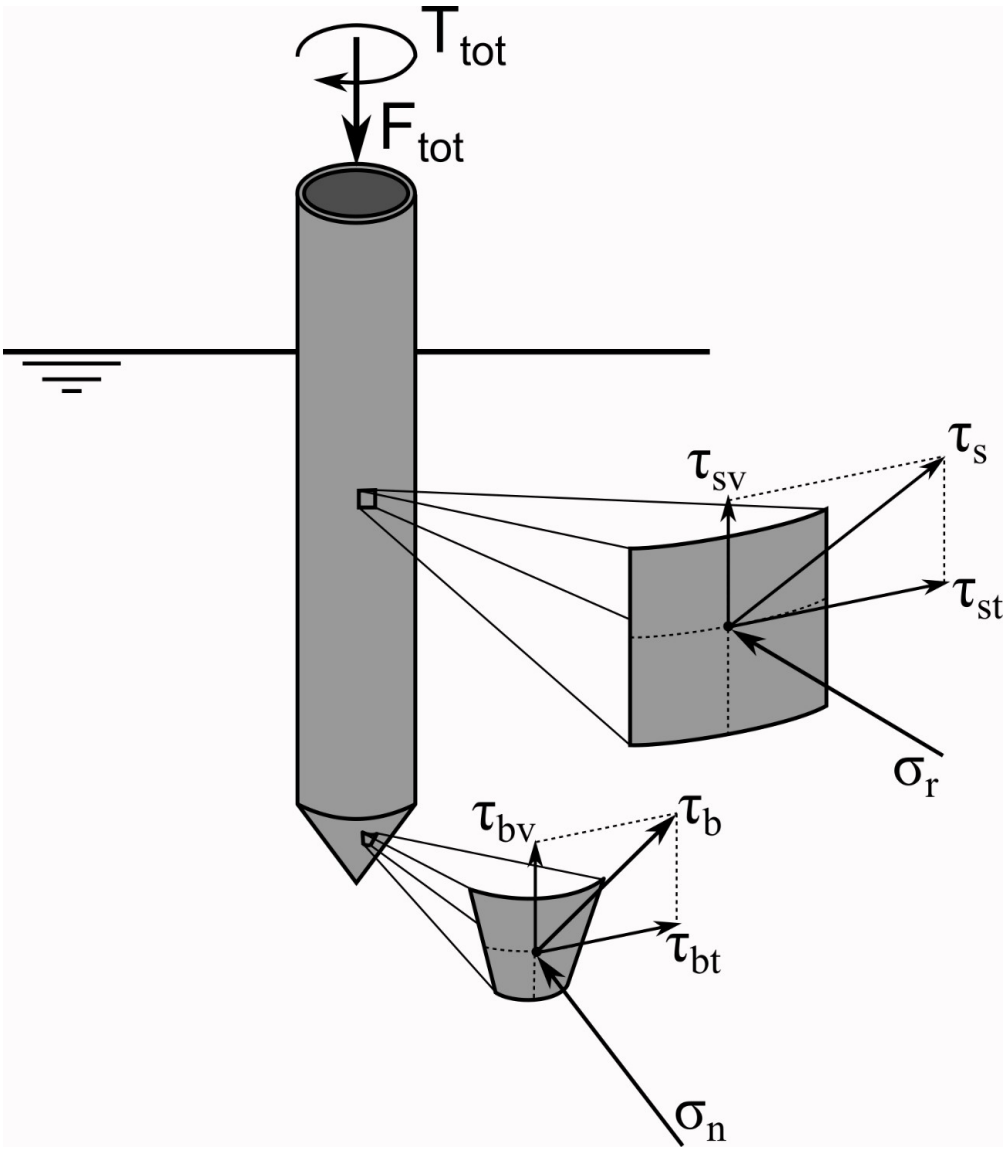

Figure 4: Schematic diagram of a rotary installed pile, showing the component and direction of shear stresses acting on a straight shafted pile during rotary installation.

149x170mm (220 x 220 DPI)

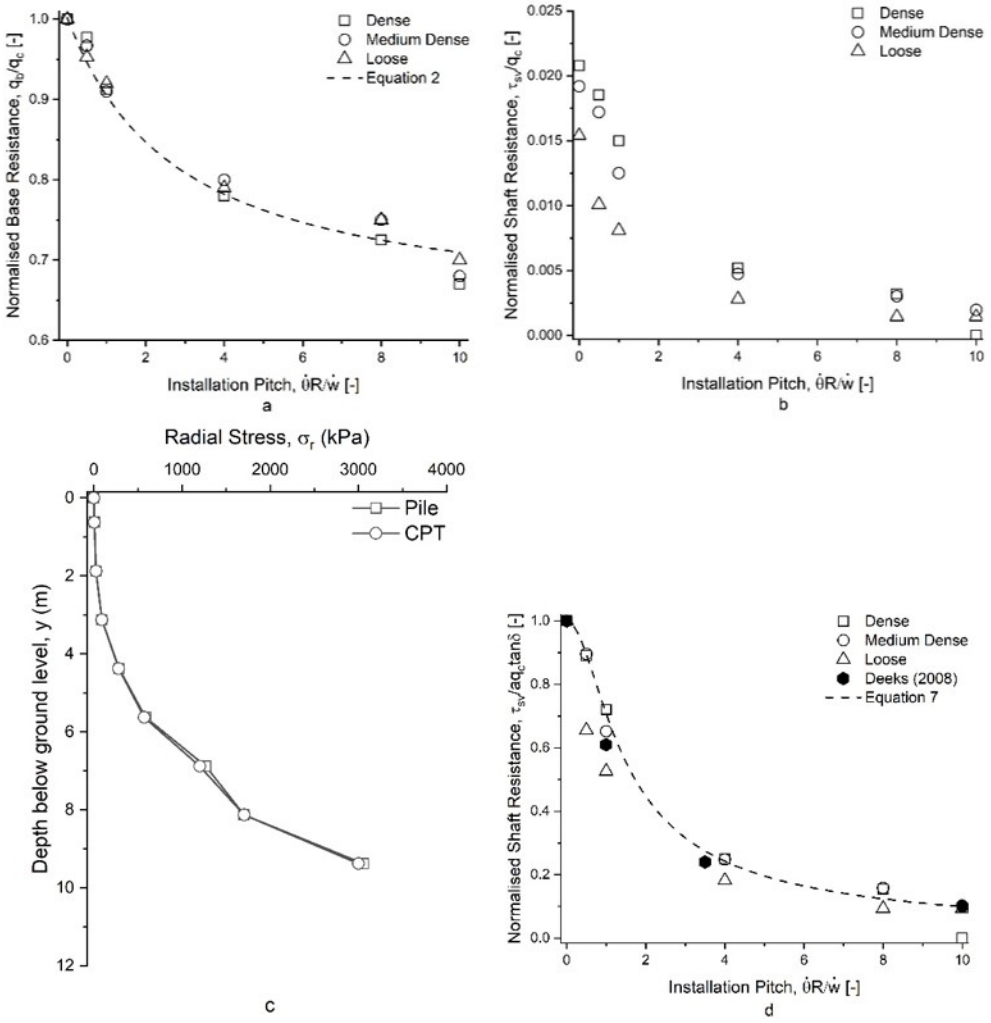

Figure 5: Comparison of normalised vertical stress results versus increasing installation pitch a) normalised base resistance (q_b/q_c) b) Normalised shaft resistance (τ_{sv}/q_c) c) Comparison of the radial stress distribution along the shaft of an installed pile and CPT in the dense soil bed (D_r = 73%) d) Comparison of equation 7 to the normalised shaft resistance from DEM and independent centrifuge tests of Deeks (2008).

132x140mm (150 x 150 DPI)

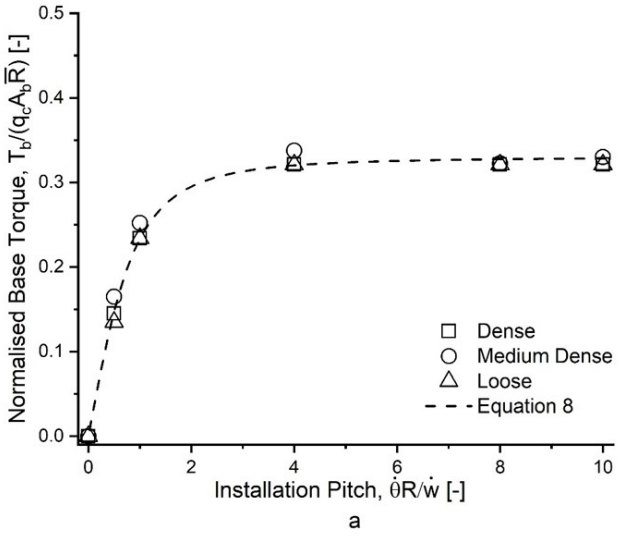

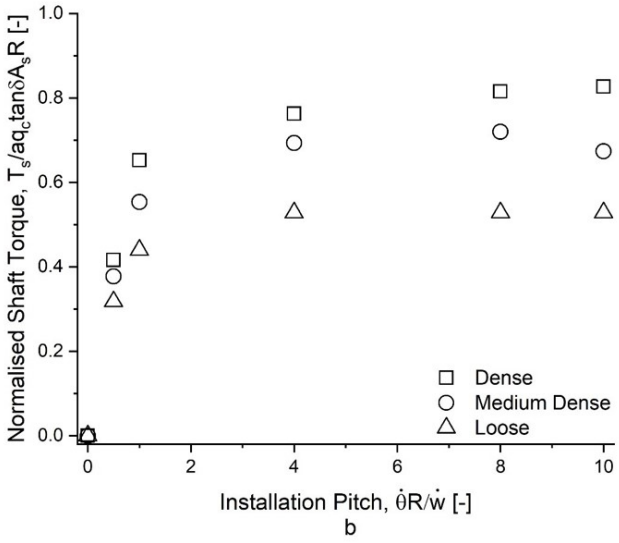

Figure 6: Normalised installation torque vs installation pitch a) base component of torque b) shaft component of torque

144x219mm (150 x 150 DPI)

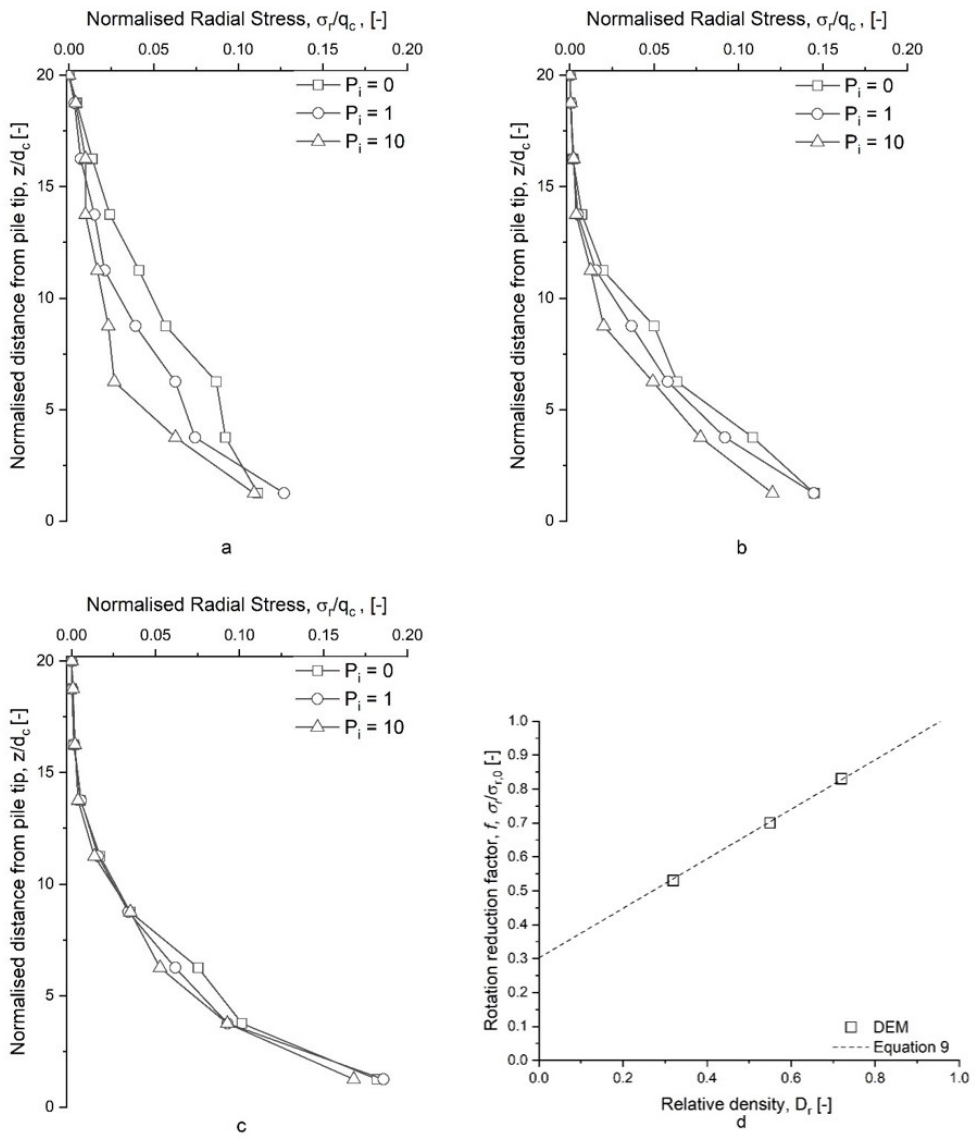

Figure 7: Comparison of normalised radial stress on the pile shaft for various installation pitches a) loose b) medium dense c) dense d) Rotation reduction factor for radial stress on the pile shaft vs relative density

155x177mm (150 x 150 DPI)

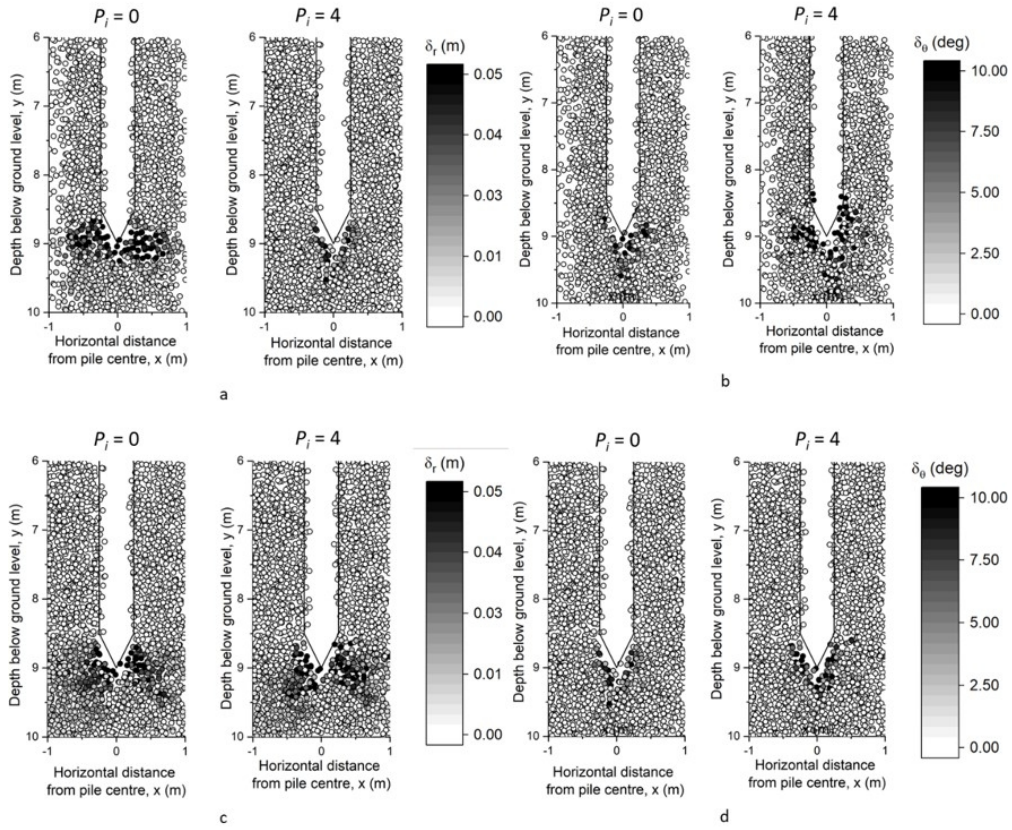

Figure 8: Comparison of particle displacement during installation at P_i = 0 & 4 for 0.25m of pile vertical movement. (Particles are shaded by displacement in polar axis) a) Loose soil bed radial displacement b) Loose soil bed rotational displacement c) Dense soil bed radial displacement d) Dense soil bed rotational displacement

149x126mm (150 x 150 DPI)

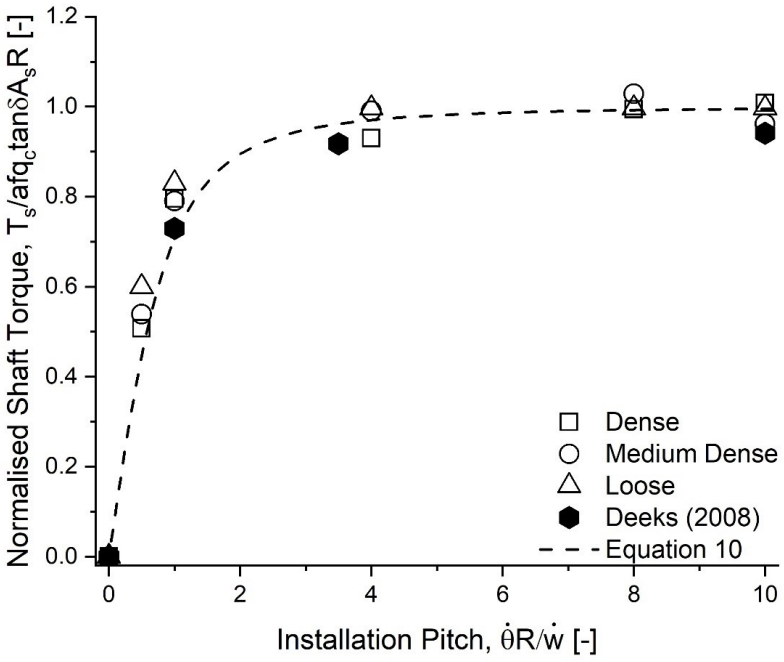

Figure 9: Comparison of normalised shaft resistance from DEM and independent centrifuge test of Deeks (2008), with the inclusion of the rotation reduction factor, to Equation 10

159x121mm (220 x 220 DPI)

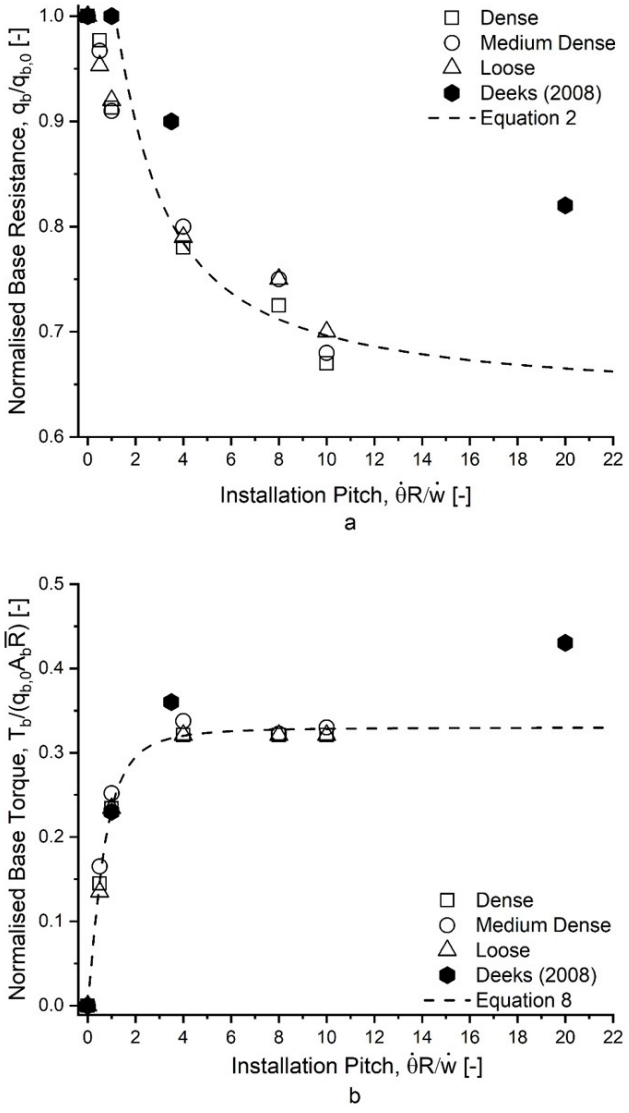

Figure 10: Comparison of base component of installation requirements between DEM and independent centrifuge tests of Deeks (2008) a) Installation force b) Installation torque

143x219mm (150 x 150 DPI)

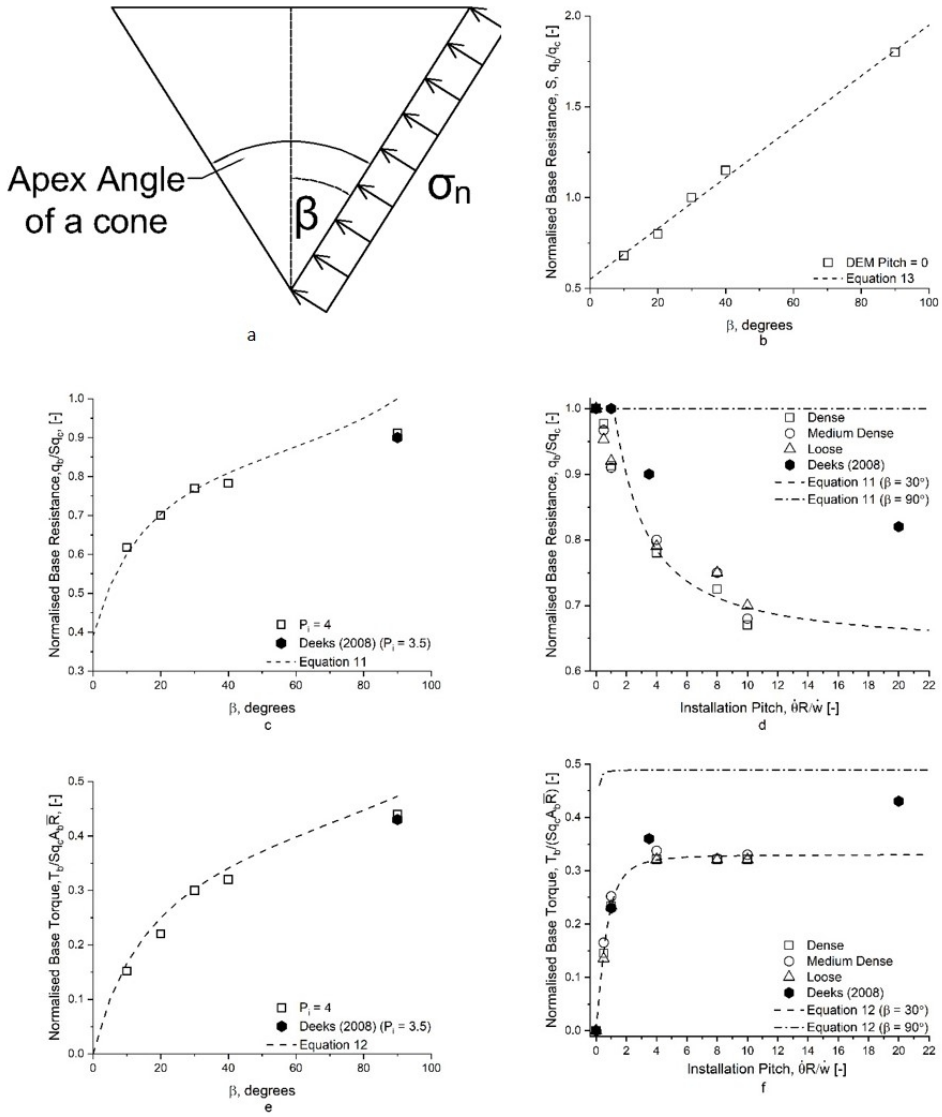

Figure 11: Comparison of Equation 11 and 12 to DEM and independent centrifuge tests of Deeks (2008) a) Diagram of possible tip geometries b) normalised base resistance for pushed in pile with different base geometries c) normalised base resistance against pile tip angle,β d) normalised base resistance against installation pitch e) normalised base torque against pile tip angle, β f) normalised base torque against installation pitch.

158x180mm (150 x 150 DPI)

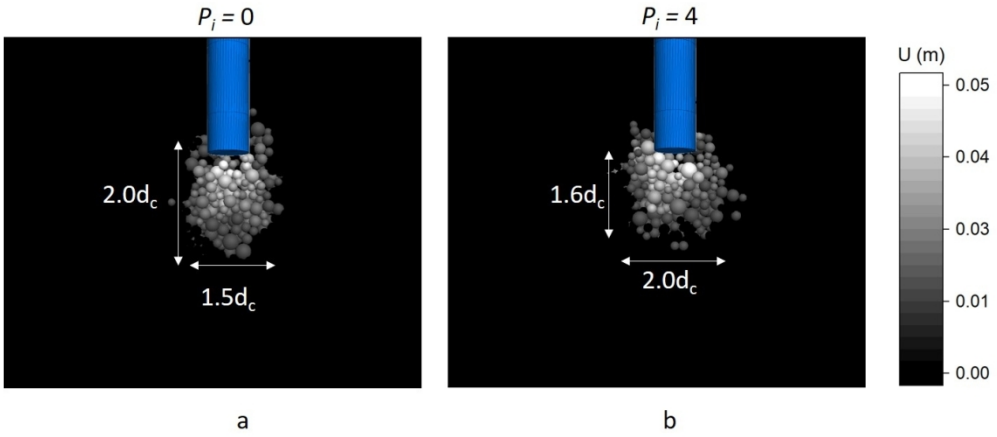

Figure 12 Average particle displacement below the base of an advancing flat based pile. a) Installation pitch = 0, b) Installation pitch = 4.

239x110mm (150 x 150 DPI)

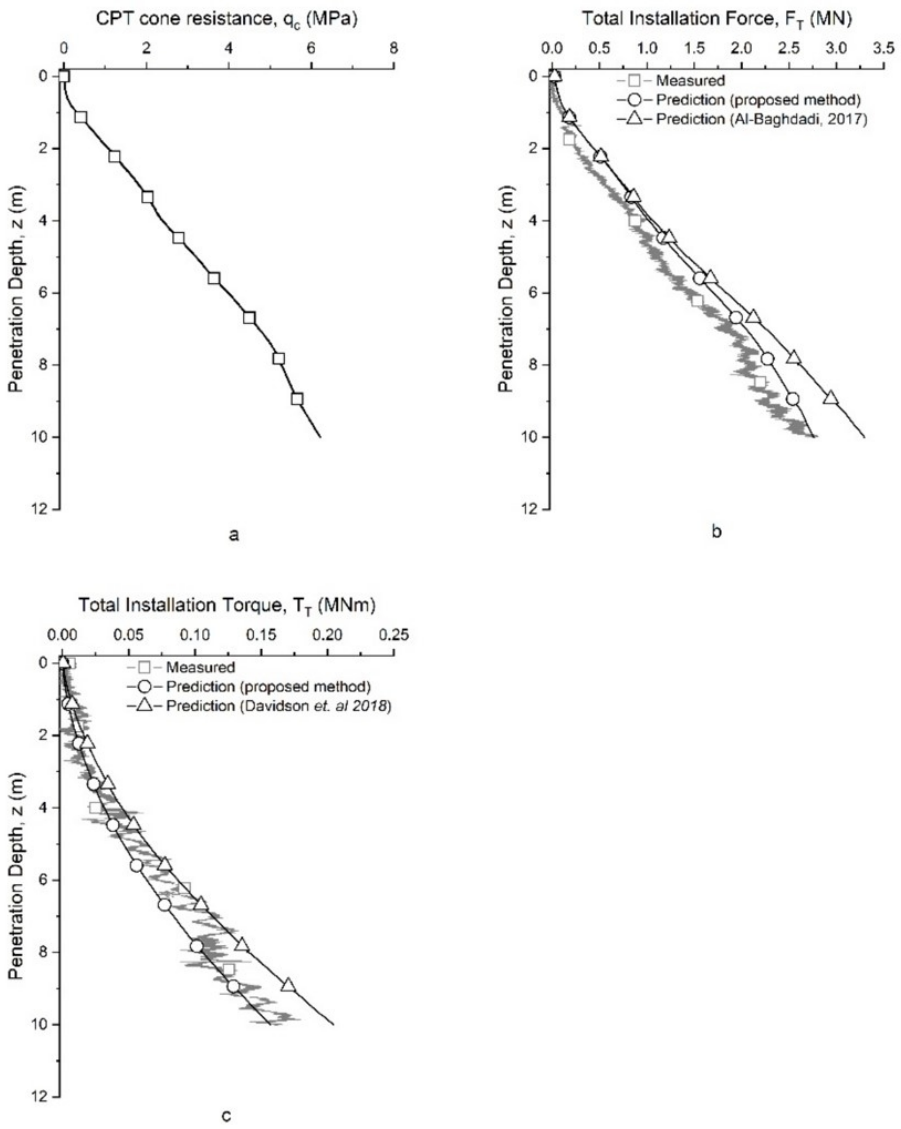

Figure 13: Prediction of installation requirements of a rotary installed straight shafted pile. Installed at P_i = 3.97 in centrifuge test from CPT Cone tip resistance, a) CPT Cone tip resistance from CPT conducted in the geotechnical centrifuge (D_r = 55%), b) Predicted vs measured prototype installation force, c) Predicted vs measured prototype Installation torque.

150x183mm (150 x 150 DPI)